

A robust neuromorphic vision sensor with optical control of ferroelectric switching

Jianyu Du^{a,b,1}, Donggang Xie^{a,c,1}, Qinghua Zhang^a, Hai Zhong^a, Fanqi Meng^a, Xingke Fu^a, Qinchao Sun^a, Hao Ni^c, Tao Li^d, Er-jia Guo^{a,b}, Haizhong Guo^e, Meng He^a, Can Wang^{a,b,f}, Lin Gu^{a,b,f}, Xiulai Xu^{a,b,f}, Guangyu Zhang^{a,b,f}, Guozhen Yang^a, Kuijuan Jin^{a,b,f,*}, Chen Ge^{a,b,*}

^a Beijing National Laboratory for Condensed Matter Physics, Institute of Physics, Chinese Academy of Sciences, Beijing 100190, China

^b University of Chinese Academy of Sciences, Beijing 100049, China

^c College of Science, China University of Petroleum (East China), Qingdao 266580, China

^d Center for Spintronics and Quantum System, State Key Laboratory for Mechanical Behavior of Materials, School of Materials Science and Engineering, Xi'an Jiaotong University, Xi'an 710049, China

^e Key Laboratory of Material Physics, Ministry of Education, School of Physics and Microelectronics, Zhengzhou University, Zhengzhou 450001, China

^f Songshan Lake Materials Laboratory, Dongguan, Guangdong 523808, China

ARTICLE INFO

Keywords:

Neuromorphic vision sensor
Ferroelectric switching
Optoelectronic synapse
2D/ferroelectric heterostructure
Interface

ABSTRACT

The rapid development of the artificial intelligence field has increased the demand for retina-inspired neuromorphic vision sensors with integrated sensing, memory, and processing functions. Here, we present a neuromorphic vision sensor with an optoelectronic transistor structure consisting of monolayer molybdenum disulfide and barium titanate ferroelectric film. Beyond conventional electrical tuning of ferroelectric polarization, the optoelectronic transistor can exhibit a light-dosage tunable synaptic behavior with a high switching ratio and good non-volatility, enabled by photo-induced ferroelectric polarization reversal. The wavelength-dependent optical sensing and multi-level optical memory properties are utilized to achieve the in-sensor neuromorphic visual pre-processing. A simulated artificial neural network built from the proposed vision sensors with neuromorphic pre-processing function demonstrated that the image recognition rate for the Modified National Institute of Standards and Technology (MNIST) handwritten dataset could be significantly improved by reducing redundant data. The obtained results suggest that 2D semiconductor/ferroelectric optoelectronic transistors can provide a promising hardware implementation towards constructing high-performance neuromorphic visual systems

1. Introduction

With the rapid development of artificial intelligence technology, the requirements of smart systems for artificial vision systems have increased [1]. An artificial vision system mainly consists of three units including the perception unit that receives optical information and converts it into digital signals, the storage unit that stores visual information, and the processing unit that performs image processing tasks [2]. However, the data storing and transferring processes performed by the three units generate large amount of unstructured and redundant data, which significantly reduces processing speed and increases power consumption [3]. These problems become even more severe in

delay-sensitive application scenarios, such as real-time video analysis and autonomous vehicle driving [4]. Thus, there is an urgent demand to develop artificial vision sensors for integrating sensing, memory, and preprocessing functions. Compared to conventional artificial vision systems, the human visual system is adept at processing unstructured data for classification and recognition. A large amount of visual information can be acquired by the human retina, and the distinctive feature can be extracted to reduce redundant data and accelerate the recognition processing in the human brain [5–7]. Inspired by the human retina, neuromorphic vision sensors combining the functions of sensing and synaptic features have been proposed to process massive data efficiently. These devices allow the data generation, storage, and computation tasks

* Corresponding authors at: Beijing National Laboratory for Condensed Matter Physics, Institute of Physics, Chinese Academy of Sciences, Beijing 100190, China.
E-mail addresses: kjjin@iphy.ac.cn (K. Jin), gechen@iphy.ac.cn (C. Ge).

¹ These authors contributed equally.

to be performed inside the sensor to reduce or eliminate data movement, thus reducing energy consumption, and improving efficiency [1,4].

Atomically thin two-dimensional (2D) transition metal dichalcogenide materials are regarded as promising candidates for the future artificial vision system [8–11]. Recently, 2D materials-based devices have been proposed to perform visual data pre-processing, such as contrast enhancement, edge enhancement, and others [2,12–14]. In addition to the mentioned aspects, there is much room for improvement in the switching ratio and non-volatile storage capacity of the artificial vision devices [12,13]. Ferroelectric materials have been widely used in non-volatile memory due to their intrinsic spontaneous polarization, and the ferroelectric field-effect transistors have been considered as potential candidates for a new type of semiconductor storage due to their low voltage operation, small cell size, and excellent non-volatility [15–18]. The heterostructures consisting of 2D direct bandgap materials and ferroelectric oxides provide an opportunity for the application of ferroelectric field-effect transistors in nonvolatile memories, neuromorphic device, and visual receptors [19–23]. Recently, Li et al. [24] reported an optically induced polarization switching phenomenon in the exfoliated multi-layer MoS₂/BTO heterostructures. Luo et al. [25]

reported an optoelectronic synapse in the exfoliated multilayer WS₂/PbZr_{0.2}Ti_{0.8}O₃ heterostructures. However, image recognition with neuromorphic preprocessing using 2D/ferroelectric optoelectronic synapses has not been explored.

In this work, a neuromorphic vision sensor based on an optoelectronic transistor using a monolayer MoS₂ channel atop a ferroelectric BTO film is presented. Due to the optical control of ferroelectric switching, the device shows light-tunable synaptic functions. We found that the optical induced switching ratio in the present device can be significantly improved compared with that in the multilayer WS₂/PbZr_{0.2}Ti_{0.8}O₃ heterostructures. In addition, the optoelectronic transistor exhibits light information extracting and multi-level optical memory properties, which are utilized in the in-sensor neuromorphic visual pre-processing. By using the optoelectronic transistors as vision sensors, a simulated artificial neural network with neuromorphic preprocessing and image recognition function is constructed. The image recognition rate on the Modified National Institute of Standards and Technology (MNIST) handwritten dataset can be greatly improved from 15% to 91% by reducing redundant data via neuromorphic preprocessing. This work shows that neuromorphic vision sensors based on

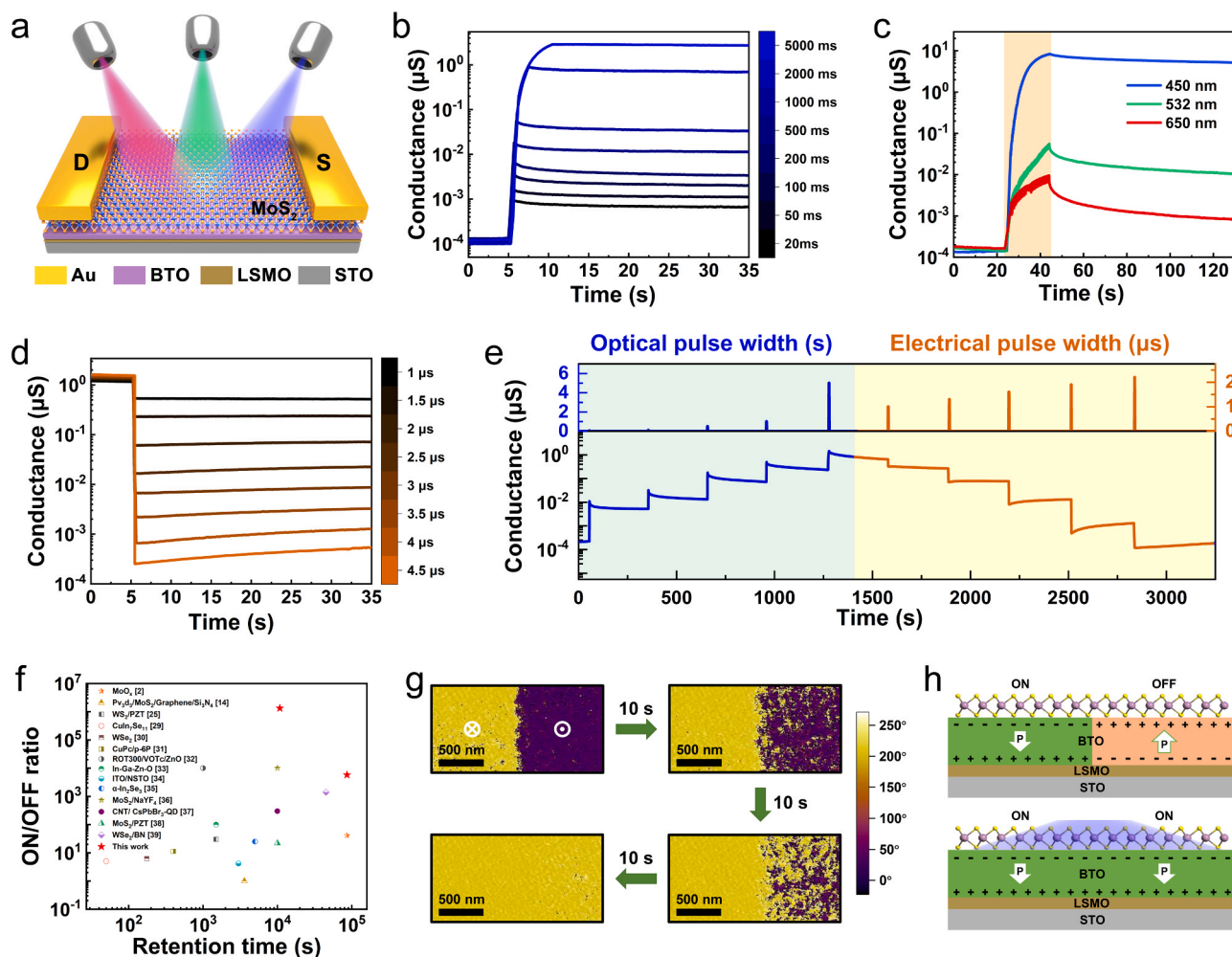


Fig. 1. Optical sensing and non-volatile multi-level memory in MoS₂/BTO transistors. (a) Schematic illustration of optoelectronic synapses stimulated by three types of light pulses (wavelengths of 450 nm, 532 nm, and 650 nm). (b) Optical-controlled conductance response of the optoelectronic transistor under optical stimuli (wavelength of 450 nm, intensity of 10 mW/cm²) with different pulse widths. (c) The conductance variation as a function of time under different light wavelengths (light intensity of 10 mW/cm², pulse number of 100). (d) Electrical-triggered conductance change of the optoelectronic transistor. The voltage pulse of 5 V was applied to the BTO layer. (e) The non-volatile multi-level conductance switching under optical excitation (pulse widths of 50 ms, 100 ms, 500 ms, 1000 ms and 5000 ms, light intensity of 10 mW/cm²) and electrical excitation (pulse widths of 1 μs, 1.3 μs, 1.6 μs, 1.9 μs and 2.2 μs). The applied voltage was fixed at 5 V. (f) Summary of the ON/OFF ratio and retention time for various optoelectronic synapses reported previously and the device in this work. (g) The PFM phase diagrams of the MoS₂/BTO heterostructure as a function of the light exposure time (wavelengths of 450 nm, intensity of approximately 5 mW/cm²). (h) Schematic diagram of the photo-induced polarization switching in the BTO film underneath the monolayer MoS₂.

2D semiconductor/ferroelectric optoelectronic transistors can provide new opportunities for the development of high-performance neuromorphic visual systems.

2. Results and discussion

The configuration of a hybrid optoelectronic synapse that consists of a monolayer MoS₂ film as a light-sensitive channel, a BTO film as a ferroelectric gate, and a La_{0.8}Sr_{0.2}MnO₃ (LSMO) film as a back electrode is presented in Fig. 1a. In this work, a large-area monolayer MoS₂ film with a direct-gap feature grown by the chemical vapor deposition (CVD) technique is used to demonstrate the potential of array preparation. The BTO and LSMO films were fabricated on SrTiO₃ (STO) substrate using the pulsed laser deposition (PLD) technique [26]. X-ray diffraction (XRD) and scanning transmission electron microscopy (STEM) results have demonstrated a high crystalline quality of the BTO/LSMO epitaxial heterostructure (Fig. S1a and c). The polarization-electric field (*P-E*) hysteresis loop in Fig. S1b shows good ferroelectric properties of BTO film. The transfer procedure of monolayer MoS₂ on the BTO films was confirmed by the atomic force microscope (AFM), Raman, and photoluminescence (PL) characterizations (Fig. S2). The successful transfer of large-area monolayer MoS₂ could be of great value for the practical application. Then, Au drain and source electrodes with a 20 μm wide and 3 μm long channel were patterned on the MoS₂/BTO heterostructures, and an Al₂O₃ insulating layer with a thickness of 60 nm was grown to reduce the leakage current. Details of the film grown and the fabrication process of the optoelectronic transistors are given in the Experimental Section and Fig. S3. The cross section image of the final transistor was shown in Fig. S4.

Next, the optoelectronic synapse behavior of the device, which could be programmed by optical pulses, was read out by the electrical operations and then investigated. The optical sensing and multi-level conductance states of the device under optical stimuli (wavelength of 450 nm, intensity of 10 mW/cm²) at different pulse widths are presented in Fig. 1b. It should be noted that the optical-induced channel states showed good non-volatility. When the pulse width changed from 20 ms to 5000 ms, the programmed channel states gradually switched from the insulating state with the conductance of approximately 7×10^{-4} μS to the more conductive state with the conductance of approximately 3 μS. Subsequently, the dependence of the optical-induced conductance state on the light intensity was investigated under different wavelengths. The conductance response was plotted as a function of time for various light intensities, and the peak value of the conductance response curve after light stimulating was summarized as a function of light intensity (Fig. S5). The conductance dependence on the light intensity exhibited a good linear relation, which is a necessary prerequisite for conductance encoding of the light information. The programmed states of the device highly depended on the light-dosage and light-history, which allowed us emulating the essential features of synaptic plasticity.

The dependence of the light-induced conductance states was further examined on the light wavelengths (Fig. 1c). Light pulses with different wavelengths of 450 nm (blue), 532 nm (green), and 650 nm (red) were used to simulate the device. The light intensity of 10 mW/cm² and the pulse number of 100 were fixed to investigate the effect of the light wavelength. When the wavelength changed to 450 nm, 532 nm, and 650 nm, the channel conductance after 100 pulses increased up to approximately 8 μS, 5×10^{-2} μS, and 9×10^{-3} μS and was stable on approximately 5 μS, 1×10^{-2} μS, and 8×10^{-4} μS after 80 s, respectively. The relaxation of the conductance can be accounted on the persistent photoconductivity (PPC) in MoS₂, which is a widely observed phenomenon in 2D transition metal dichalcogenide [25]. When the light wavelength changed from 650 nm to 450 nm, an enhancement of almost four orders of magnitude in the channel conductance was observed after light illumination, suggesting high sensitivity of the proposed optoelectronic transistor to blue light. The difference in photoresponse could

be attributed to the difference in optical absorption coefficient with photon energy [27]. To investigate the memory retention dependence on the wavelengths, the memory retention (*MR*) was calculated as follows [7,25]:

$$MR = (G_t - G_{\text{off}}) / (G_{\text{max}} - G_{\text{off}}) \quad (1)$$

where G_t denotes the conductance change with time, G_{off} is the initial conductance value, and G_{max} is the maximum conductance value. The Kohlrausch stretched-exponential function was used to fit the decay behavior of the light-induced conductance response as follows [28]:

$$MR \sim \exp\left[-(t/\tau)^\beta\right] \quad (2)$$

where τ denotes the characteristic relaxation time, which represents the non-volatile characteristic, and β is the stretch index.

The *MR* characteristic of the optical-induced conductance response was analyzed. The *MR* values obtained from Fig. 1c were plotted as a function of time and fitted by Eq. (2), as shown in Fig. S6. When the wavelength varied from 650 nm to 450 nm, the relaxation time τ increased from 3 s to 416 s, indicating good non-volatile behavior for the proposed optoelectronic transistor under blue light. This result implies that the proposed optoelectronic transistors can be applied to neuromorphic vision sensors to extract and store blue light information.

Not only the long-term potentiation (LTP) behavior of biological synapses could be modeled by applying optical pulses on the device, but also the long-term depression (LTD) behavior could be emulated by using electrical pulses. When a voltage pulse (5 V) exceeding the coercive voltage of the ferroelectric film was applied to the BTO layer, the channel conductance decreased with the increase in the electrical pulse width and recovered to the initial state at the electrical pulse width of 4.5 μs (Fig. 1d). To verify the performance of the proposed optoelectronic transistors applied to neuromorphic computing, the multi-level conductance states, which were triggered by both optical and electrical pulses, were further demonstrated (Fig. 1e). In the process of the blue-light-triggered potentiation, the optical pulses with different durations (50 ms, 100 ms, 500 ms, 1000 ms, and 5000 ms) were applied to the device. The channel conductance measured after removing the light exhibited long retention of 300 s. During the electrical-triggered depression, the voltage pulses with different widths (1 μs, 1.3 μs, 1.6 μs, 1.9 μs, and 2.2 μs) were applied to the BTO film. The applied voltage was fixed at 5 V, which exceeded the coercive voltage of the BTO film. The retention properties of the device was investigated by using optical potentiation (wavelength of 450 nm, width of 10 s) and electrical depression (voltage of 5 V, width of 100 ms), as shown in Fig. S7. The distinct states retain a ratio of 2×10^7 within 3600 s, and a ratio of 6×10^3 after 86,400 s. The reliability of the device was investigated by using optical potentiation (wavelength of 450 nm, width of 10 s) and electrical depression (voltage of 5 V, width of 100 ms) to switch the device between high- and low-conductance states (Fig. S8). No endurance degradation occurred after 100 switching cycles. Compared with those of the previous works [2,14,25,29–40], the present MoS₂/BTO optoelectronic synapse exhibits an excellent memory performance with a high ON/OFF ratio and a long retention time (Fig. 1f). The superior performance of the MoS₂/BTO/LSMO heterostructures mainly originates from the monolayer MoS₂ with atomic-thickness, the high quality BTO film with suitable thickness, and a clean interface between the BTO and MoS₂.

To explore the underlying mechanism behind the optical-induced synaptic functions in the MoS₂/BTO optoelectronic transistors, the PFM measurements were performed after illumination at different times (Fig. 1g). By applying ±5 V bias to the tip, the MoS₂-covered BTO was set into downward polarization state (left) and upward polarization state (right), respectively. Then, the whole region was illuminated by three light pulses (wavelength of 450 nm, intensity of 5 mW/cm², width of 10 s). After each stimulation, the same region of the device was

scanned in the dark. With the increase in the exposure time, the polarization of MoS₂-covered BTO gradually switched into a downward state, while the region with the initial downward polarization state did not change after the light illumination (Fig. 1h). To exclude the possibility that the region of upward polarization could spontaneously tend to be polarized downward in MoS₂/BTO heterostructures, a control experiment was performed without illumination processes (Fig. S9). The result indicated that the original upward polarization state remained stable for at least an hour without illumination. To exclude the influence of persistent photoconductivity (PPC) effect induced by the trapping charges, the monolayer MoS₂ based transistor was fabricated on the substrate of doped Si covered by 300-nm thick thermal SiO₂ [25,41]. Although the MoS₂/SiO₂/Si-based transistor exhibited finite non-volatile memory behavior, the switching ratio of approximately two was much lower than that of the BTO-based transistor, which was more than 10⁷, as shown in Fig. S10. The measurement results confirmed the dominant role of optical-controlled ferroelectric switching in the proposed optoelectronic synaptic device, which is consistent with the recent works using exfoliated 2D flakes/ferroelectric structures [25]. The light-controlled ferroelectric polarization switching can be explained in terms of the interaction between the photogenerated charges in MoS₂ and ferroelectric polarization charges in BTO, according to the recently proposed theory [24]. Due to the MoS₂/BTO/SRO heterojunction are essentially asymmetric, P_{down} is the preferred polarization state over the opposite one, which is equivalent to the presence of the built-in field E_{bi} oriented toward the bottom electrode. The photogenerated positive charge accumulation at the MoS₂/BTO interface screens the upward polarization, which leads to the polarization reversal by the built-in electric field E_{bi} [24]. The ferroelectric polarization switching process strongly depends on the light-dosage, and the multi-level conductance states under different light-dosage can be ascribed to the mixed ferroelectric domain states with various ratios of upward and downward ferroelectric domains. By electrically tuning the mixed ferroelectric

domain states, the conductance state can gradually recover to the initial state. The experimental results clearly indicate that the proposed device has the integrated optical-sensing capability and synaptic functions, which are essential features of neuromorphic vision sensors.

It's worth noting that the device states cannot transform from the low conductance state to the high conductance state through applying the negative voltage. This is mainly attributed to its highly insulating state of the MoS₂ channel when BTO is in the upward polarization. Previous study showed that the spreading of ferroelectric layer polarization is not directly by the fringing field from the top electrode, but by the 2D TMD layer that functions as a conductive pad to enhance the fringing field to pole the ferroelectric layer underneath [21]. Therefore, after the BTO film was set into upward polarization and the MoS₂ channel turned into the OFF state, the domain switching would be difficult to spread out.

The integrated image detection and memorization of the proposed device were demonstrated on a 5 × 5 array (Fig. 2). Before the write operation, each unit in the array was pre-reset to the low conductance state by applying a voltage pulse (5 V, width of 100 ms) to the BTO layer (Fig. 2a). Two types of stimuli were applied to the array for implementing the photoelectrical information storage. One was a series of light pulses, including the blue light stimuli (wavelength of 450 nm, intensity of 10 mW/cm², width of 100 ms, 30 pulses) and red light stimuli (wavelength of 650 nm, intensity of 10 mW/cm², width of 100 ms, 30 pulses); the other one is a voltage pulse (5 V, width of 100 ms). As shown in Fig. 2b, the image of "X" was written to the vision sensor array by applying the blue light stimuli to the MoS₂ channel. After the light stimuli, the conductance of the vision sensor greatly increased. In this work, there are two erase/write operations for the vision sensor array, namely "electrical erasing - optical writing" and "optical erasing - electrical writing". The "electrical erasing - optical writing" mode is presented in Fig. 2c. The image of "X" was electrically erased by individually switching the ferroelectric polarization upward to reset the

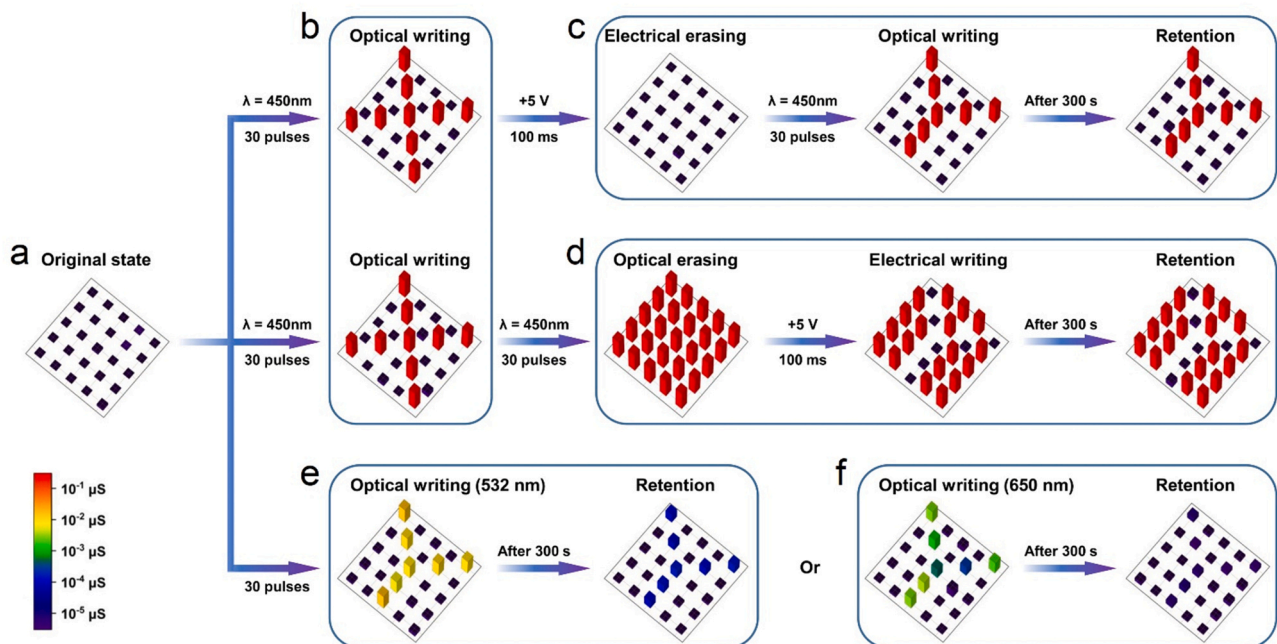


Fig. 2. Image detection and memorization in a vision sensor array. A 5 × 5 MoS₂/BTO optoelectronic synapse array constructed as a neuromorphic vision sensor to implement the image sensing and memorization functions. A series of the optical pulses and the electrical pulse (5 V for 100 ms) applied to the array to mimic the writing and erasing operations. The conductance was read at 10 s after the light pulse stimuli. (a) Before optical stimuli, all devices are in the low-conductance state. (b) The initial image of "X" was written to the vision sensor array using the optical pulse train (wavelength of 450 nm, number of 30, intensity of 10 mW/cm², width of 100 ms duration and interval of 100 ms). (c) The process of "electrical erasing - optical writing" mode. (d) The process of "optical erasing - electrical writing" mode. (e) The image of "Y" was written by applying a series of the optical pulse (wavelength of 532 nm, number of 30, intensity of 10 mW/cm², width of 100 ms, and interval of 100 ms) and the retention characteristic was also investigated after 5 min (f) The image of "Y" was written by applying a series of the optical pulse (wavelength of 650 nm, number of 30, intensity of 10 mW/cm², width of 100 ms and interval of 100 ms). The retention characteristic was measured after 300 s.

conductance of device units. Then, the image of “Y” was written optically by the blue light stimulus train, and the image of “Y” was visible even after 300 s, indicating an excellent memorization feature. The “optical erasing - electrical writing” mode is presented in Fig. 2d. The image of “X” was electrically erased by blue light stimulus train and the image of “Y” was written electrically by the electrical pulse. Compared to the “electrical erasing - optical writing” mode, the “optical erasing - electrical writing” mode could simultaneously erase the original information by setting all devices to the high-conductance state by light illumination instead of individually switching the ferroelectric polarization upward. This mode is suitable for handling large-scale data erasure tasks, and the same task can take several times longer if every memory unit is reset individually. By applying the green and red light stimulus train, the image of “X” can also be written to the array as shown in Fig. 2e and f, but the photoelectric response decayed significantly, especially for the writing with red light stimulus train. The experimental results further prove that the proposed device has high sensitivity and good non-volatile behavior for blue light. For exploring the minimum of

the power consumption, we tested the device using the power density $30 \mu\text{W}/\text{cm}^2$ and the illumination time 100 ms (Fig. S11). The energy consumption per synaptic event of optically stimulated synaptic devices can be calculated by using $dE=S \times P \times dt$ [42], where S is the area of the channel, P is the power density of the light illumination, t is the duration time of light. The energy consumption per synaptic event of the device is 1.8 pJ. Even so, further works definitely need to be done to improve the light response efficiency.

In image recognition, the extraction of useful light information can significantly reduce the interference of redundant information and improve the speed of subsequent signal processing effectively [43]. Therefore, the extracting the efficacious information from the original optical information is one of the most important functions for object identification in an intelligent vision system, which is essential in the application of visual information preprocessing [44–46].

Based on the integrated optical-sensing capability and high sensitivity of the proposed device to blue light, a neuromorphic vision sensor array was simulated to realize image preprocessing. The extraction of

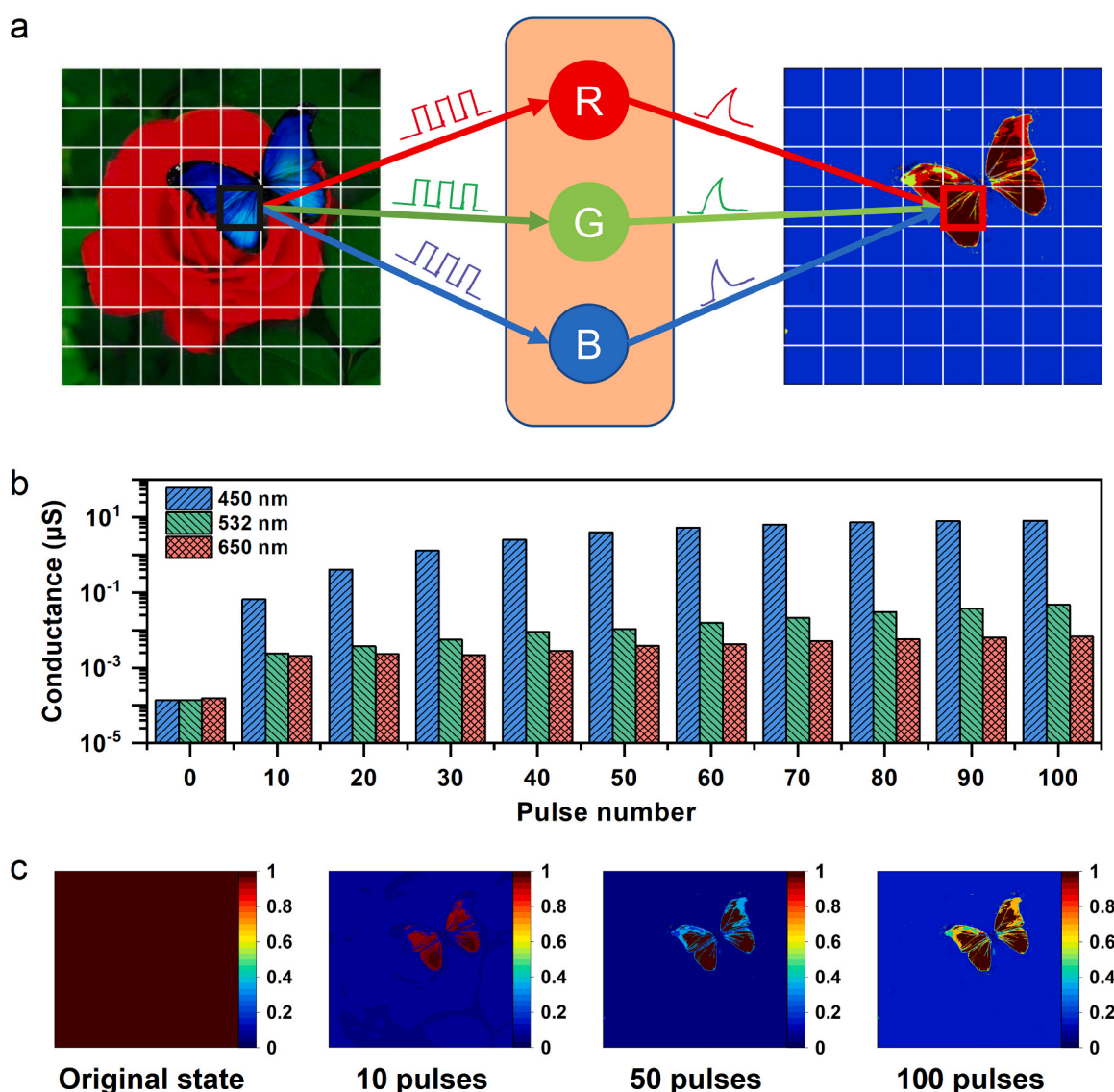


Fig. 3. Implementation of color information extraction using the neuromorphic vision sensor array. (a) A schematic image of encoding the color information into the corresponding photocurrent intensity. (b) Statistics of the channel conductance as a function of pulse number in the neuromorphic vision sensor device under different light pulses, namely red (red columns), green (green columns), and blue (blue columns) light pulses. The light intensity and the number of pulse were fixed at $10 \text{ mW}/\text{cm}^2$ and 100, respectively. The duration and interval were both 100 ms. The encoding result of conductance was normalized and mapped. (c) The difference between the blue and other features with the increase in the pulse number.

blue signals was conducted by using the proposed sensor array (Fig. 3a). Before the color image was fed to the array, the red (R), green (G), and blue (B) components were sampled (Fig. S12a-c). From the sampled images, the features of flower, leaves, and butterfly were most obvious in R, G, and B images, respectively. In order to send these three sampled images to the sensor array, the values of R, G, and B were mapped to the intensity of the light pulses having the wavelengths of 650 nm, 532 nm, and 450 nm, respectively (Fig. S12d-f). The dependence of the light-induced conductance state on the pulse numbers under different wavelengths is presented in Fig. 3b. The fixed light intensity of 10 mW/cm² was used to investigate the effect of the pulse number, and the output image was represented by the device conductance. As the pulse number increased, the feature of a butterfly whose characteristic color is blue was highlighted, and the most obvious butterfly was observed after 100 pulses (Figs. 3c and S12g-l). This result indicates that the contrast between the blue features and the other features can be enhanced by increasing the pulse number, and the proposed sensor array could efficiently recognize the blue targets. The detailed process of the color image preprocessing is described in Supplementary Note 1.

To examine the bio-vision inspired neuromorphic computation, a simulated visual system, including the proposed neuromorphic vision sensor array and an artificial neural network (ANN), was designed. In this system, the sensor array acted as a preprocessing part to extract and store the blue information, while the ANN acted as an image recognition part to recognize the blue information offered by the former (Fig. S13). It is worth mentioning that the image recognition part was also constructed based on the extracted device parameters, that is, each synaptic weight (w) and bias (b) in the ANN were determined by a pair of normalized conductance values [47] (Figs. S14 and S15, and Table S1). The schematic of the human visual system is displayed in Fig. 4a. The visual information was first accepted by the human eyes and then pre-processed by a variety of cells in the retina. The visual information with obvious characteristics was transmitted to the visual cortex of the brain for final image recognition. In the neuromorphic visual system, the real image was sampled into three components of R, G, and B. After the RGB images were sent to the sensor array, the output image with less redundant information and obvious characteristics was sent to the three-layer ANN for subsequent image recognition (Fig. 4b and c).

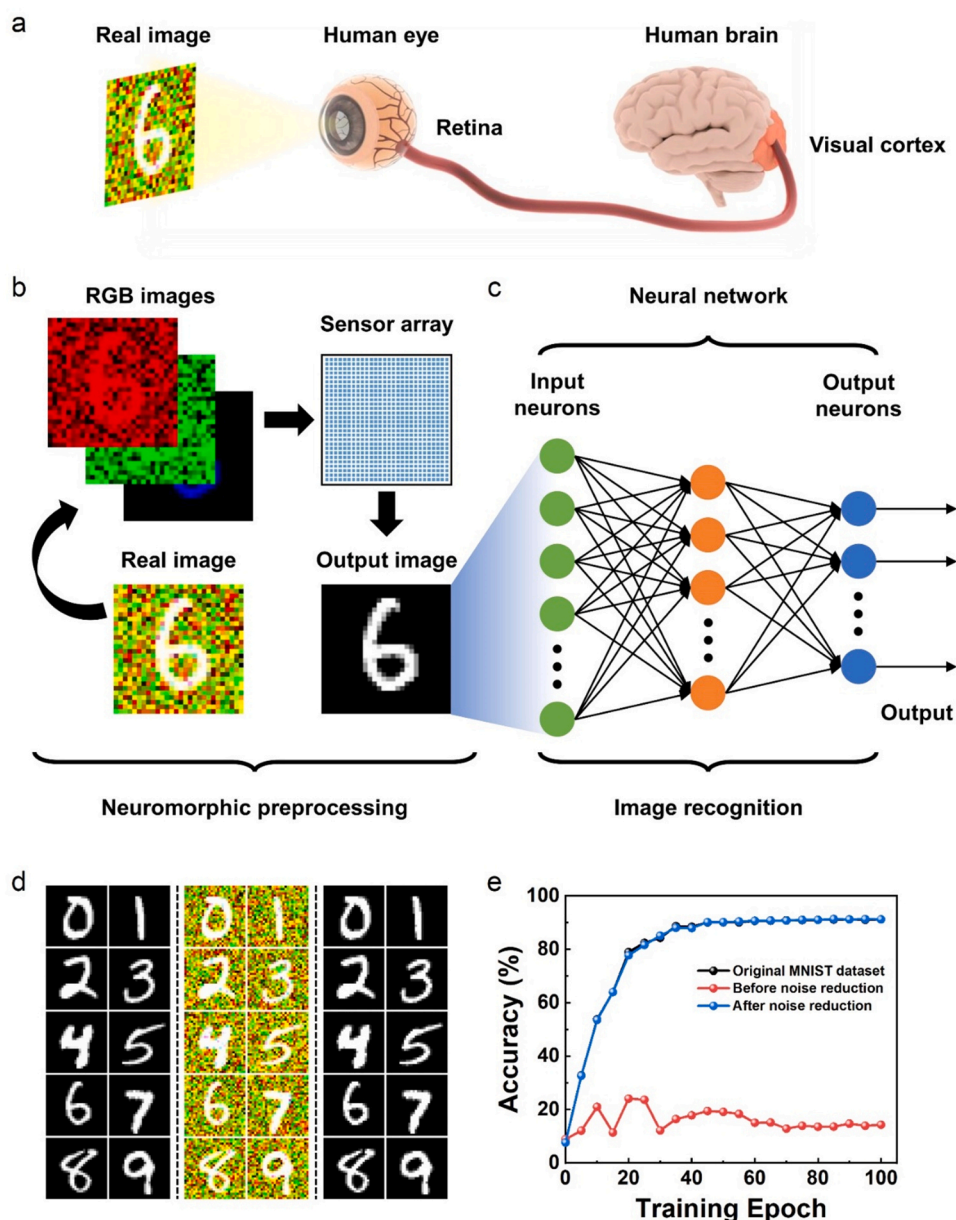


Fig. 4. Image recognition in the MoS₂/BTO optoelectronic synapse-based neuromorphic visual system. (a) Schematics of the human visual recognition system. (b) The preprocess of the image noise reduction utilizing the sensor array. (c) Illustration of the image recognition using artificial neural network. (d) Three types of pre-prepared images including the original MNIST test images (left columns), the specially processed images with R&G Gaussian noise (middle columns), and the images after noise reduction by the sensor array (right columns). (e) Comparisons of the recognition accuracy of the pre-prepared images.

Specially processed data were used as the input to verify the reliability of the proposed device in preprocessing. These data were the MNIST test dataset [48] consisting of 10,000 images with a size of 28×28 pixels each, which were added with red and green (R&G) Gaussian noise signals. In Fig. 4b, one of the real images is presented. Afterward, the real image was sampled into three images, which were RGB images. As the sampled RGB images were sent to the sensor array (one real image pixel corresponded to one device), the optical signals were converted into device conductance, as explained above. Then, the output image could be read out by the voltage. The image information contained in the output image was subsequently normalized and sent to the ANN having an input layer (784), a hidden layer (300), and an output layer (10) for image recognition (Fig. 4c). The detailed operation mechanism of the ANN is described in Supplementary Note 2. The network was trained by the back-propagation algorithm [49] using 60,000 images from the MNIST train dataset, and the recognition accuracy of 10 digits was achieved by using three types of pre-prepared images: the original MNIST test images, the specially processed images with R&G Gaussian noise, and the images after noise reduction of the sensor array. These pre-prepared images are shown in Fig. 4d. The dependence of the recognition accuracy on the training epoch number for different types of images is shown in Fig. 4e. The recognition accuracy of the dataset before noise reduction could reach only about 15% after 100 epochs, which was marginally higher than the initial accuracy, suggesting that the ANN can hardly recognize this type of dataset. In contrast, the recognition accuracies of the other types of the datasets were perfectly consistent, reaching about 90% after 45 epochs, and about 91% after 100 epochs, which were significantly higher than that of the dataset before noise reduction. This result indicates that the preprocessing of the proposed sensor array can effectively extract feature information and reduce redundant data, thus the subsequent image recognition unit can accurately recognize the visual information that was originally unrecognizable. The performance of the proposed neuromorphic visual system and previously reported systems are summarized in Table S2, showing the excellent capability of the proposed system in the neuromorphic preprocessing for specific tasks. The successful demonstrations of neuromorphic preprocessing and image recognition suggest that the proposed neuromorphic visual system can be brilliantly applied in the complex color image recognition, and the neuromorphic vision sensors based on 2D semiconductor/ferroelectric optoelectronic transistors can provide new opportunities for the development of high-performance neuromorphic visual systems.

3. Conclusions

In summary, we successfully fabricated the $\text{MoS}_2/\text{BaTiO}_3$ optoelectronic synapse with monolayer MoS_2 as the light-sensitive channel and BTO film as the ferroelectric gate, and demonstrated its integrated optical sensing and multi-level optical memory functions, which are promising for neuromorphic vision sensors. Beyond conventional electrical tuning of the ferroelectric domain, the optoelectronic transistor with a high optical memory switching ratio and a long retention time can exhibit light-dosage tunable synaptic behaviors. Moreover, we show that this type of device has the potential to be fabricated into an array. The non-volatile multi-level conductance states can be ascribed to the optical controlled mixed states with various ratios of upward and downward ferroelectric domains. It has been found that the synaptic properties can also be significantly manipulated by electrical gating. An artificial neural network is built from the proposed vision sensors, and results demonstrate that the image recognition rate on the MNIST handwritten dataset has been increased from 15% to 91% by reducing redundant data using the neuromorphic pre-processing process. It should be noted that the material composition in the proposed device can be generalized to a broad range of 2D semiconductors and ferroelectrics. This work provides the potential to fabricate the large-scale array consisting of ferroelectric optoelectronic synapses that could be

promising for creating advanced neuromorphic vision systems.

4. Methods

4.1. Material preparation

Pulsed laser deposition (PLD) using a XeCl excimer laser with a wavelength of 308 nm and a repetition rate of 2 Hz was employed to fabricate BTO (~ 40 nm) and LSMO (~ 10 nm) heterostructures on (001) SrTiO_3 substrates. The BTO and LSMO films were deposited at 750°C and cooled down to room temperature of $20^\circ\text{C min}^{-1}$ in a flowing oxygen atmosphere of 20 Pa. The deposition rate of the oxide films was calibrated by X-ray Reflection (XRR) technique. The large-scale ($1\text{ cm} \times 1\text{ cm}$) MoS_2 monolayer was synthesized by chemical vapor deposition (CVD) on the SiO_2/Si substrate and then transferred to the top of the BTO layer.

4.2. Device fabrication

The transferred MoS_2 was patterned into channels using standard photolithography and reaction ion-beam etching (RIBE). A $20\ \mu\text{m}$ wide and $3\ \mu\text{m}$ long channel was delimited by Au drain (~ 100 nm) and the source electrode. Before depositing the electrodes, a $60\ \text{nm Al}_2\text{O}_3$ insulation layer, which was sandwiched between the BTO layer and Au electrodes, was prepared through magnetron sputtering for reducing the leakage current.

4.3. Sample characterization

X-ray diffraction measurements were performed using a Rigaku SmartLab instrument. A commercial scanning probe microscope (Asylum Research MFP3D) with a contact PtIr-coated silicon tip was used to measure the PFM amplitude and phase image. A ferroelectric tester (Radiant Technologies, Premier II) was used to acquire the ferroelectric hysteresis loop in the Pt/BTO/LSMO structure at 10 kHz. The cross-sectional images were recorded by an ARM-200F (JEOL, Tokyo, Japan) scanning transmission electron microscope. Raman and photoluminescence (PL) spectrum of the transferred MoS_2 on BTO film was analyzed using the alpha300 R microscope under 532 nm laser excitation.

4.4. Electrical measurement

The electronic and optoelectronic measurements were conducted using a Lake Shore TTPX cryogenic probe station connected with a Keithley 4200 semiconductor parameter analyzer in vacuum at room temperature. The source-drain voltage was fixed at $-0.1\ \text{V}$ during all the measurements. The optoelectronic measurements were performed by using semiconductor lasers with various wavelengths of 450 nm, 532 nm and 650 nm. A computer-controlled shutter was utilized to manipulate the light pulse widths and intervals. The illumination power was measured and calibrated by GCI-08 photodetector (Daheng Optics).

CRedit authorship contribution statement

Jianyu Du: Investigation, Formal analysis, Writing – original draft, Writing – review & editing, Validation. **Donggang Xie:** Formal analysis, Writing – original draft, Writing – review & editing, Validation, Software. **Qinghua Zhang, Fanqi Meng, Lin Gu:** Characterization. **Hai Zhong, Xingke Fu, Qincao Sun, Hao Ni, Tao Li, Er-jia Guo, Haizhong Guo, Meng He, Can Wang, Xiulai Xu, Guangyu Zhang:** Investigation, Writing – review & editing. **Guozhen Yang:** Resources, Writing – review & editing. **Kuijuan Jin:** Resources, Writing – review & editing, Funding acquisition. **Chen Ge:** Conceptualization, Supervision, Project administration, Funding acquisition, Writing – review & editing.

Declaration of Competing Interest

The authors declare that they have no known competing financial interests or personal relationships that could have appeared to influence the work reported in this paper.

Acknowledgments

Jianyu Du and Donggang Xie contributed equally to this work. This work was supported by the National Key R&D Program of China (No. 2017YFA0303604 and 2019YFA0308500), the Youth Innovation Promotion Association of CAS (No. 2018008), the National Natural Science Foundation of China (Nos. 12074416, 11674385, 11404380, 11721404, and 11874412), and the Key Research Program of Frontier Sciences CAS (No. QYZDJSSW-SLH020).

Author contributions

Chen Ge initiated the research and supervised the project. The samples were grown by Hai Zhong; The devices were fabricated by Jianyu Du and Hai Zhong; Device measurements were carried out by Jianyu Du and Xingke Fu; Simulations of image recognition with pre-processing were performed by Donggang Xie; PFM were performed by Jianyu Du and Qincao Sun; XRD, Raman, and PL measurements were performed by Jianyu Du; STEM experiments were performed by Qinghua Zhang, Fanqi Meng, and Lin Gu. Chen Ge, Jianyu Du, and Donggang Xie wrote the manuscript. All authors participated in the discussion of manuscript.

Appendix A. Supporting information

Supplementary data associated with this article can be found in the online version at [doi:10.1016/j.nanoen.2021.106439](https://doi.org/10.1016/j.nanoen.2021.106439).

References

- [1] F. Zhou, Y. Chai, Near-sensor and in-sensor computing, *Nat. Electron.* 3 (2020) 664–671.
- [2] F. Zhou, Z. Zhou, J. Chen, T.H. Choy, J. Wang, N. Zhang, Z. Lin, S. Yu, J. Kang, H.-S.P. Wong, Y. Chai, Optoelectronic resistive random access memory for neuromorphic vision sensors, *Nat. Nanotechnol.* 14 (2019) 776–782.
- [3] L. Mennel, J. Symonowicz, S. Wächter, D.K. Polyushkin, A.J. Molina-Mendoza, T. Mueller, Ultrafast machine vision with 2D material neural network image sensors, *Nature* 579 (2020) 62–66.
- [4] Y. Chai, In-sensor computing for machine vision, *Nature* 579 (2020) 32–33.
- [5] G. Wang, R. Wang, W. Kong, J. Zhang, Simulation of retinal ganglion cell response using fast independent component analysis, *Cogn. Neurodyn* 12 (2018) 615–624.
- [6] H. Wang, Q. Zhao, Z. Ni, Q. Li, H. Liu, Y. Yang, L. Wang, Y. Ran, Y. Guo, W. Hu, Y. Liu, A ferroelectric/electrochemical modulated organic synapse for ultraflexible, artificial visual-perception system, *Adv. Mater.* 30 (2018), 1803961.
- [7] T. Ohno, T. Hasegawa, T. Tsuruoka, K. Terabe, J.K. Gimzewski, M. Aono, Short-term plasticity and long-term potentiation mimicked in single inorganic synapses, *Nat. Mater.* 10 (2011) 591–595.
- [8] N. Li, Q. Wang, C. Shen, Z. Wei, H. Yu, J. Zhao, X. Lu, G. Wang, C. He, L. Xie, J. Zhu, L. Du, R. Yang, D. Shi, G. Zhang, Large-scale flexible and transparent electronics based on monolayer molybdenum disulfide field-effect transistors, *Nat. Electron.* 3 (2020) 711–717.
- [9] V.K. Sangwan, H.-S. Lee, H. Bergeron, I. Balla, M.E. Beck, K.-S. Chen, M.C. Hersam, Multi-terminal memtransistors from polycrystalline monolayer molybdenum disulfide, *Nature* 554 (2018) 500–504.
- [10] S.-G. Kim, S.-H. Kim, J. Park, G.-S. Kim, J.-H. Park, K.C. Saraswat, J. Kim, H.-Y. Yu, Infrared detectable MoS₂ phototransistor and its application to artificial multilevel optic-neural synapse, *ACS Nano* 13 (2019) 10294–10300.
- [11] S. Seo, S.-H. Jo, S. Kim, J. Shim, S. Oh, J.-H. Kim, K. Heo, J.-W. Choi, C. Choi, S. Oh, D. Kuzum, H.-S.P. Wong, J.-H. Park, Artificial optic-neural synapse for colored and color-mixed pattern recognition, *Nat. Commun.* 9 (2018) 5106.
- [12] C.-Y. Wang, S.-J. Liang, S. Wang, P. Wang, Z. Li, Z. Wang, A. Gao, C. Pan, C. Liu, J. Liu, H. Yang, X. Liu, W. Song, C. Wang, B. Cheng, X. Wang, K. Chen, Z. Wang, K. Watanabe, T. Taniguchi, J.J. Yang, F. Miao, Gate-tunable van der Waals heterostructure for reconfigurable neural network vision sensor, *Sci. Adv.* 6 (2020) 6173.
- [13] T. Ahmed, M. Tahir, M.X. Low, Y. Ren, S.A. Tawfik, E.L.H. Mayes, S. Kuriakose, S. Nawaz, M.J.S. Spencer, H. Chen, M. Bhaskaran, S. Sriram, S. Walia, Fully light-controlled memory and neuromorphic computation in layered black phosphorus, *Adv. Mater.* 33 (2021), 2004207.
- [14] C. Choi, J. Leem, M.S. Kim, A. Taqieddin, C. Cho, K.W. Cho, G.J. Lee, H. Seung, H. J. Bae, Y.M. Song, T. Hyeon, N.R. Aluru, S. Nam, D.-H. Kim, Curved neuromorphic image sensor array using a MoS₂-organic heterostructure inspired by the human visual recognition system, *Nat. Commun.* 11 (2020) 5934.
- [15] X. Chai, J. Jiang, Q. Zhang, X. Hou, F. Meng, J. Wang, L. Gu, D.W. Zhang, A. Q. Jiang, Nonvolatile ferroelectric field-effect transistors, *Nat. Commun.* 11 (2020) 2811.
- [16] R. Guo, L. You, W. Lin, A. Abdelsamie, X. Shu, G. Zhou, S. Chen, L. Liu, X. Yan, J. Wang, J. Chen, Continuously controllable photoconductance in freestanding BiFeO₃ by the macroscopic flexoelectric effect, *Nat. Commun.* 11 (2020) 2571.
- [17] M. Carroli, A.G. Dixon, M. Herder, E. Pavlica, S. Hecht, G. Bratina, E. Orgiu, P. Samorì, Multiresponsive nonvolatile memories based on optically switchable ferroelectric organic field-effect transistors, *Adv. Mater.* 33 (2021), 2007965.
- [18] X. Long, H. Tan, F. Sánchez, I. Fina, J. Fontcuberta, Non-volatile optical switch of resistance in photoferroelectric tunnel junctions, *Nat. Commun.* 12 (2021) 382.
- [19] Z.-D. Luo, M.-M. Yang, Y. Liu, M. Alexe, Emerging opportunities for 2D semiconductor/ferroelectric transistor-structure devices, *Adv. Mater.* 33 (2021), 2005620.
- [20] X. Wang, P. Yu, Z. Lei, C. Zhu, X. Cao, F. Liu, L. You, Q. Zeng, Y. Deng, C. Zhu, J. Zhou, Q. Fu, J. Wang, Y. Huang, Z. Liu, Van der Waals negative capacitance transistors, *Nat. Commun.* 10 (2019) 3037.
- [21] C. Ko, Y. Lee, Y. Chen, J. Suh, D. Fu, A. Suslu, S. Lee, J.D. Clarkson, H.S. Choe, S. Tongay, R. Ramesh, J. Wu, Ferroelectrically gated atomically thin transition-metal dichalcogenides as nonvolatile memory, *Adv. Mater.* 28 (2016) 2923–2930.
- [22] G. Wu, B. Tian, L. Liu, W. Lv, S. Wu, X. Wang, Y. Chen, J. Li, Z. Wang, S. Wu, H. Shen, T. Lin, P. Zhou, Q. Liu, C. Duan, S. Zhang, X. Meng, S. Wu, W. Hu, X. Wang, J. Chu, J. Wang, Programmable transition metal dichalcogenide homojunctions controlled by nonvolatile ferroelectric domains, *Nat. Electron.* 3 (2020) 43–50.
- [23] L. Lv, F. Zhuge, F. Xie, X. Xiong, Q. Zhang, N. Zhang, Y. Huang, T. Zhai, Reconfigurable two-dimensional optoelectronic devices enabled by local ferroelectric polarization, *Nat. Commun.* 10 (2019) 3331.
- [24] T. Li, A. Lipatov, H. Lu, H. Lee, J.-W. Lee, E. Torun, L. Wirtz, C.-B. Eom, J. Íñiguez, A. Sinitskii, A. Gruverman, Optical control of polarization in ferroelectric heterostructures, *Nat. Commun.* 9 (2018) 3344.
- [25] Z.-D. Luo, X. Xia, M.-M. Yang, N.R. Wilson, A. Gruverman, M. Alexe, Artificial optoelectronic synapses based on ferroelectric field-effect enabled 2D transition metal dichalcogenide memristive transistors, *ACS Nano* 14 (2020) 746–754.
- [26] J. Li, C. Ge, J. Du, C. Wang, G. Yang, K. Jin, Reproducible ultrathin ferroelectric domain switching for high-performance neuromorphic computing, *Adv. Mater.* 32 (2020), 1905764.
- [27] E. Yalon, Ö.B. Aslan, K.K.H. Smithe, C.J. McClellan, S.V. Suryavanshi, F. Xiong, A. Sood, C.M. Neumann, X. Xu, K.E. Goodson, T.F. Heinz, E. Pop, Temperature-dependent thermal boundary conductance of monolayer MoS₂ by Raman thermometry, *ACS Appl. Mater. Interfaces* 9 (2017) 43013–43020.
- [28] T. Chang, S.-H. Jo, W. Lu, Short-term memory to long-term memory transition in a nanoscale memristor, *ACS Nano* 5 (2011) 7669–7676.
- [29] S. Lei, F. Wen, B. Li, Q. Wang, Y. Huang, Y. Gong, Y. He, P. Dong, J. Bellah, A. George, L. Ge, J. Lou, N.J. Halas, R. Vajtai, P.M. Ajayan, Optoelectronic memory using two-dimensional materials, *Nano Lett.* 15 (2015) 259–265.
- [30] X. Hou, C. Liu, Y. Ding, L. Liu, S. Wang, P. Zhou, A logic-memory transistor with the integration of visible information sensing-memory-processing, *Adv. Sci.* (Weinh.) 7 (2020), 2002072.
- [31] C. Qian, S. Oh, Y. Choi, J.-H. Kim, J. Sun, H. Huang, J. Yang, Y. Gao, J.-H. Park, J. H. Cho, Solar-stimulated optoelectronic synapse based on organic heterojunction with linearly potentiated synaptic weight for neuromorphic computing, *Nano Energy* 66 (2019), 104095.
- [32] H. Wang, H. Liu, Q. Zhao, Z. Ni, Y. Zou, J. Yang, L. Wang, Y. Sun, Y. Guo, W. Hu, Y. Liu, A retina-like dual band organic photosensor array for filter-free near-infrared-to-memory operations, *Adv. Mater.* 29 (2017), 1701772.
- [33] W. Qiu, Y. Huang, L.-A. Kong, Y. Chen, W. Liu, Z. Wang, J. Sun, Q. Wan, J.H. Cho, J. Yang, Y. Gao, Optoelectronic In-Ga-Zn-O memtransistors for artificial vision system, *Adv. Funct. Mater.* 30 (2020), 2002325.
- [34] S. Gao, G. Liu, H. Yang, C. Hu, Q. Chen, G. Gong, W. Xue, X. Yi, J. Shang, R.-W. Li, An oxide schottky junction artificial optoelectronic synapse, *ACS Nano* 13 (2019) 2634–2642.
- [35] F. Xue, X. He, W. Liu, D. Periyanaounder, C. Zhang, M. Chen, C. Lin, L. Luo, E. Yengel, V. Tung, T.D. Anthopoulos, L. Li, J. He, X. Zhang, Optoelectronic ferroelectric domain-wall memories made from a single van Der Waals ferroelectric, *Adv. Funct. Mater.* 30 (2020), 2004206.
- [36] Y. Zhai, X. Yang, F. Wang, Z. Li, G. Ding, Z. Qiu, Y. Wang, Y. Zhou, S.-T. Han, Infrared-sensitive memory based on direct-grown MoS₂-upconversion-nanoparticle heterostructure, *Adv. Mater.* 30 (2018), 1803563.
- [37] Q.-B. Zhu, B. Li, D.-D. Yang, C. Liu, S. Feng, M.-L. Chen, Y. Sun, Y.-N. Tian, X. Su, X.-M. Wang, S. Qiu, Q.-W. Li, X.-M. Li, H.-B. Zeng, H.-M. Cheng, D.-M. Sun, A flexible ultrasensitive optoelectronic sensor array for neuromorphic vision systems, *Nat. Commun.* 12 (2021) 1798.
- [38] A. Lipatov, P. Sharma, A. Gruverman, A. Sinitskii, Optoelectrical molybdenum disulfide (MoS₂)-ferroelectric memories, *ACS Nano* 9 (2015) 8089–8098.
- [39] D. Xiang, T. Liu, J. Xu, J.Y. Tan, Z. Hu, B. Lei, Y. Zheng, J. Wu, A.H.C. Neto, L. Liu, W. Chen, Two-dimensional multibit optoelectronic memory with broadband spectrum distinction, *Nat. Commun.* 9 (2018) 2966.
- [40] F. Zhou, J. Chen, X. Tao, X. Wang, Y. Chai, 2D materials based optoelectronic memory: convergence of electronic memory and optical sensor, *Research* (Washington, D.C.) 2019 (2019), 9490413.

- [41] H.-K. He, R. Yang, W. Zhou, H.-M. Huang, J. Xiong, L. Gan, T.-Y. Zhai, X. Guo, Photonic potentiation and electric habituation in ultrathin memristive synapses based on monolayer MoS₂, *Small* 14 (2018), 1800079.
- [42] Z. Ni, Y. Wang, L. Liu, S. Zhao, Y. Xu, X. Pi, D. Yang, Hybrid structure of silicon nanocrystals and 2D WSe₂ for broadband optoelectronic synaptic devices, in: 2018 IEEE International Electron Devices Meeting (IEDM), ieeexplore.ieee.org, 2018: pp. 38.5.1–38.5.4.
- [43] H.-L. Park, H. Kim, D. Lim, H. Zhou, Y.-H. Kim, Y. Lee, S. Park, T.-W. Lee, Retina-inspired carbon nitride-based photonic synapses for selective detection of UV light, *Adv. Mater.* 32 (2020), 1906899.
- [44] R.D. Jansen-van Vuuren, A. Armin, A.K. Pandey, P.L. Burn, P. Meredith, Organic photodiodes: the future of full color detection and image sensing, *Adv. Mater.* 28 (2016) 4766–4802.
- [45] J. Xue, Z. Zhu, X. Xu, Y. Gu, S. Wang, L. Xu, Y. Zou, J. Song, H. Zeng, Q. Chen, Narrowband perovskite photodetector-based image array for potential application in artificial vision, *Nano Lett.* 18 (2018) 7628–7634.
- [46] M. Hasantash, R. Lafer-Sousa, A. Afraz, B.R. Conway, Paradoxical impact of memory on color appearance of faces, *Nat. Commun.* 10 (2019) 3010.
- [47] M. Prezioso, F. Merrih-Bayat, B.D. Hoskins, G.C. Adam, K.K. Likharev, D. B. Strukov, Training and operation of an integrated neuromorphic network based on metal-oxide memristors, *Nature* 521 (2015) 61–64.
- [48] Y. LeCun, C. Cortes, C.J.C. Burges, The MNIST database of handwritten digits, n.d. (<http://yann.lecun.com/exdb/mnist/>).
- [49] Y. Lecun, L. Bottou, Y. Bengio, P. Haffner, Gradient-based learning applied to document recognition, *Proc. IEEE Inst. Electr. Electron. Eng.* 86 (1998) 2278–2324.